Development of tissue-simulating optical phantoms: poly-N-isopropylacrylamide solution entrapped inside a hydrogel

Guillermo Marquez†, Lihong V Wang†, Changjie Wang‡ and Zhibing Hu‡

† Optical Imaging Laboratory, Biomedical Engineering Program, Texas A&M University, College Station, TX 77843-3120, USA
‡ Department of Physics, University of North Texas, Denton, TX 76203, USA

Abstract. The average turbid optical properties of the N-isopropylacrylamide (NIPA) polymer solution entrapped inside a polyacrylamide hydrogel (called an NIPA/PAAM gel system) were studied using a multiwavelength oblique-incidence reflectometer. The turbidity of such a system can be drastically changed by simply switching the temperature from below the low critical solution temperature of the NIPA, around 33 °C, to above. The absorption coefficient and the reduced scattering coefficient were obtained as a function of wavelength for samples with selected NIPA and blue dextran concentrations. It is found that the scattering of the optical phantom comes from the NIPA polymer chains and the absorption from the blue dextran. The turbid optical properties of an NIPA/PAAM gel system can be tuned to simulate biological tissues at a specific wavelength by varying compositions of NIPA and blue dextran and further modified by controlling the temperature.

1. Introduction

In both diagnostic and therapeutic applications of light in medicine, it is important to evaluate optical properties of biological tissues including the absorption coefficient and the reduced scattering coefficient (Pickering *et al* 1993). One of the challenges in this area is to develop tissue-simulating turbid media (optical phantoms). Optical phantoms may be used to test and calibrate optical instruments or techniques. A typical optical phantom with static optical properties consists of deionized water mixed with minimally scattering Trypan blue dye as the absorbers and minimally absorbing polystyrene spheres as the scatterers (Wang and Jaques 1995).

In this study we report a new optical phantom with dynamic optical properties that consists of an entrapped poly-N-isopropylacrylamide (PNIPA) polymer solution and a host matrix of a polyacrylamide (PAAM) hydrogel. The PAAM hydrogel is transparent in the temperature range (Tanaka 1992) in which this study was carried out, and holds the NIPA solution so that the solution can be easily transported and handled in the laboratory. The NIPA polymer solution undergoes a phase transition from a hydrophilic to a hydrophobic structure rather abruptly at the lower critical solution temperature (LCST) (Schild 1992). Below the LCST NIPA is transparent, and above the LCST it becomes cloudy. The advantage of such an optical phantom is that its turbidity can be tuned reversibly by simply varying the temperature. For a neutral NIPA polymer solution, this LCST is found to be about 32 °C (Schild 1992, Schild and Tirrell 1990). By copolymerizing NIPA with acrylamide over the entire composition range,

Taylor and Cerankowski (1975) and Priest *et al* (1987) found that the LCST can go either up or down when the comonomer has respectively a smaller or larger group. Such an ability to shift the LCST of NIPA-like polymers provides excellent flexibility in tailoring the transition for a specific use (Schild 1992).

As a temperature-responsive turbid medium the NIPA/PAAM gel system has the potential to be used to simulate dynamically varying turbid optical properties of biological tissues at a specific wavelength. For example, photocoagulation of biological tissues varies the optical properties of the tissues as the coagulation progresses. Current optical phantoms have static optical properties, which may not be varied once the phantoms are made. The new temperature-responsive phantoms will have unique advantages for this type of simulation. Here, the average turbid optical properties of the NIPA/PAAM gel system are characterized using a multiwavelength oblique-incidence reflectometer.

2. Experiment

2.1. Sample preparation

The samples were prepared in two steps. First, the NIPA polymer solution was obtained using free radical polymerization (Schild 1992). A mixture of 7.8 g of N-isopropylacrylamide and tetra-methyl-ethylene-diamine (240 μl) as an accelerator were dissolved in 100 ml of deionized and distilled water. Nitrogen gas was bubbled through the solution to remove dissolved oxygen. Then 40 mg ammonium persulfate (APS) was added to the solution as an initiator. The gelation process was completed in about 30 min. The sample was left in the reactor overnight. Second, the NIPA solution was introduced into a pre-gel solution of acrylamide (PAAM). After mixing these two solutions, the cross-linker and the initiator were added to form the PAAM gel with the entrapped NIPA solution. The chemical composition of the PAAM gel was obtained using the NIPA recipe with the 7.8 g of N-isopropylacrylamide monomers replaced by 5 g of acrylamide and 0.133 g of methylene-bis-acrylamide as a cross-linker. The weight ratios between the PAAM and entrapped NIPA were 1:0.1 for phantoms 1 and 2 and 1:0.5 for phantom 3. An additional amount of 0.05 g of blue dextran was mixed into phantom 2. The phantoms became opaque in either aqueous NaCl solution (>1.2 M) or a warm bath ($T > 33\,^\circ$C).

2.2. Optical experiments

The experimental system for measuring the absorption coefficient and the reduced scattering coefficient of the optical phantom is drawn schematically in figure 1. White light (Oriel, 75 W xenon arc lamp) was delivered, and the diffuse reflectance was collected with a fibre optic probe made from black Delrin and 600 μm diameter low-OH optical fibres. The source fibre was oriented at a 45° angle of incidence, and the nine collection fibres, arranged in a linear array, collected the diffuse reflectance. To correct for slight variations in collection efficiency from one detection fibre to the next, we calculated a correction factor for each fibre based on a calibration procedure using standard phantoms (Lin *et al* 1996). The detection system was composed of an imaging spectrograph (Oriel, Multispec 257), a CCD camera (Princeton Instrument Inc., 1530P) and a personal computer to automatically record the spectrum of the collected light through the wavelength range of 450–800 nm (Marquez and Wang 1997).

Phantom 1 (PAAM:NIPA 1:0.1), phantom 2 (PAAM:NIPA 1:0.1 with 0.05 g of blue dextran) and phantom 3 (PAAM:NIPA 1:0.5) were placed in a bath of water and heated to a temperature of approximately 60 $^\circ$C for 1 h until the phantoms were completely turbid. The fibre probe was aligned perpendicular to the surface of the phantoms. An exposed x-ray film
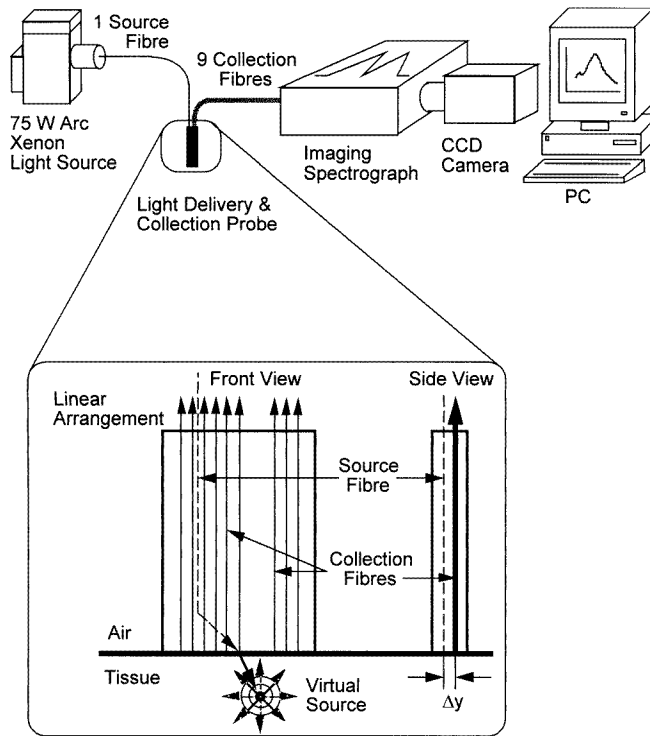
Figure 1. Schematic diagram of the experimental apparatus. White light was coupled to the oblique-incidence optical fibre probe. A source fibre delivered light to the gel phantoms at an angle of 45° and the diffuse reflectance was collected by nine collection fibres. All fibres were encased to form a hand-held probe. The angle of refraction was computed to be 46.6°. The collected diffuse reflectance was analysed and its spectrum recorded using the multiwavelength oblique incidence reflectometer (MWOIR).

was placed on top of the phantom to approximate a matched boundary condition for diffusion theory (Lin 1996). Ten reflectance measurements were performed to obtain an average value of the optical properties, which in turn improved the signal/noise ratio. The probe was moved and rotated to ten different positions on the phantom surface.

The turbidity (A) of the optical phantoms was obtained from the ratio of the transmitted light intensity (I_t) to the incident intensity (I_0), $A = -(1/L) \ln(I_t/I_0)$, where L is the length of the sample. The light transmission was measured by a spectrophotometer operating at a wavelength (λ) of 555 nm. An external water circulator controlled the temperature of the sample. In addition to the temperature sensor in the circulator, a thermocouple was placed inside the sample cell for temperature measurement. The cell was sealed using a plastic film to prevent evaporation. The accuracy of the temperature measurement was estimated to be $\pm 0.5\,^\circ$C.

3. Theory

This section summarizes, for completeness, the theory behind our optical method described in detail by Lin *et al* (1997). When light enters a semi-infinite tissue, it will generally scatter a number of times before either being absorbed or escaping the tissue. This scattered light that

escapes is called diffuse reflectance. This diffusion theory model does not accurately model 'near diffuse reflectance', i.e. reflectance that falls within the range of one to two transport mean free paths (mfps) of the source (Wang and Jaques 1993). This problem can be avoided by using only the 'far diffuse reflectance', i.e. reflectance that falls beyond the range of one to two mfps of the source.

For normally incident light, the spatial distribution of diffuse reflectance from a semi-infinite turbid medium has been modelled by two isotropic point sources: one positive source located below the tissue surface and one negative image source above the tissue surface (Farrell *et al* 1992). If light is delivered obliquely, the positive source is buried at the same distance from the point of incidence but with a depth modified by Snell's law. Wang and Jacques (1992) found the distance of the buried source to the point of incidence to be most accurately determined by

$$d_s = 3D = \frac{1}{0.35\mu_a + \mu'_s} \tag{1}$$

where D is the diffusion coefficient, μ_a the absorption coefficient and μ'_s the reduced scattering coefficient. Therefore, the fundamental difference between normal and oblique incidence is a shift in the positions of the point sources in the x direction (figure 2). This shift, Δx, is

$$\Delta x = \frac{\sin \alpha_t}{0.35\mu_a + \mu'_s} \tag{2}$$

where α_t is the angle of refraction, which may be calculated from the relative index of refraction n and the angle of incidence α_i. The relative index of refraction is unity for a matched boundary.
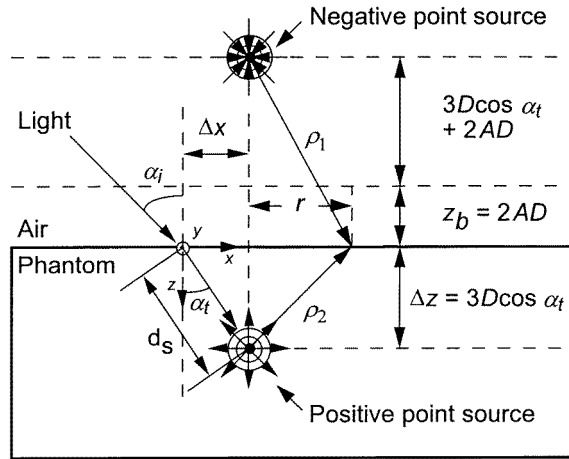
Figure 2. Schematic representation of obliquely incident light. Note the shift in the centre of diffuse reflectance, Δx. The position of the two point sources in the diffusion theory model of oblique incidence reflectometry is shown.

The modified dipole source diffusion theory model gives the diffuse reflectance

$$R(x) = \frac{1}{4\pi} \left(\frac{\Delta z(1 + \mu_{\text{eff}}\rho_1) \exp(-\mu_{\text{eff}}\rho_1)}{\rho_1^3} + \frac{(\Delta z + 2z_b)(1 + \mu_{\text{eff}}\rho_2) \exp(-\mu_{\text{eff}}\rho_2)}{\rho_2^3} \right) \tag{3}$$

where x is the distance between the point of observation and the point of light incidence, ρ_1 and ρ_2 are the distances from the two point sources to the point of interest, z_b is the distance

between the virtual boundary and the surface of the tissue

$$z_b = 2AD \tag{4}$$

where A, a parameter related to the internal reflection is unity for a matched boundary, Δz is the depth of the positive point source

$$\Delta z = \frac{\cos \alpha_t}{0.35\mu_a + \mu'_s} = \Delta x \tan^{-1} \alpha_t \tag{5}$$

and μ_{eff} is the effective attenuation coefficient

$$\mu_{\text{eff}} = \sqrt{\frac{\mu_a}{D}}. \tag{6}$$

Equation (3) can be scaled to fit a relative reflectance profile.

Therefore, the first step in our procedure was to measure the diffuse reflectance profile with our fibre optic probe. We used white light for a multiwavelength measurement. The light collected by each detection fibre was input to the imaging spectrograph for spectral resolution. Because we determine the spectrum collected by each fibre, we have in fact measured the spatial distribution of diffuse reflectance at many wavelengths simultaneously. Thus the reflectance profile at any wavelength can be extracted and analysed to deduce the optical properties at that wavelength. Lin *et al* (1996) have demonstrated that absorption and reduced scattering spectra can be easily obtained with this method and with an accuracy of 10% and 5% respectively.

Once the position of the centre of the far diffuse reflectance relative to the light entry point (Δx) was found, the diffusion coefficient was calculated from

$$D = \frac{\Delta x}{3 \sin \alpha_t}. \tag{7}$$

Then a nonlinear least squares fit to equation (3) with the Levenberg-M-arquardt method (Press *et al* 1992) yielded the effective attenuation coefficient, μ_{eff}. Equations (2), (6) and (7) were used to compute μ_a and μ'_s as follows

$$\mu_a = \frac{\mu^2_{\text{eff}} \Delta x}{\sin \alpha_t} \tag{8}$$

and

$$\mu'_s = \frac{\sin \alpha_t}{\Delta x} - 0.35\mu_a. \tag{9}$$

4. Results

A typical result of turbidity as a function of temperature is shown in figure 3 for phantom 3. It is apparent that the turbidity of the sample increased drastically as the LCST reached about 33 °C. The optical properties of the phantoms presented below were all obtained at $T = 60$ °C at which the samples are in the high turbid state.

The average turbid optical properties of phantom 1 (PAAM:NIPA 1:0.1) are plotted in figure 4. The absorption coefficient is negligible between 500 and 700 nm compared with the reduced scattering coefficient (figure 4(*a*)). The reduced scattering coefficient decreased smoothly with an increase in wavelength (figure 4(*b*)). In figure 5 we plot the average turbid optical properties of phantom 2 (PAAM:NIPA 1:0.1 with 0.05 g of blue dextran). The spectrum of the absorption coefficient, μ_a, has a maximum of 0.63 cm^{-1} at 610 nm which is typical of blue dextran (figure 5(*a*)). The reduced scattering coefficient also decreased smoothly with an increase in wavelength (figure 5(*b*)). In figure 6 we plot the average turbid optical properties
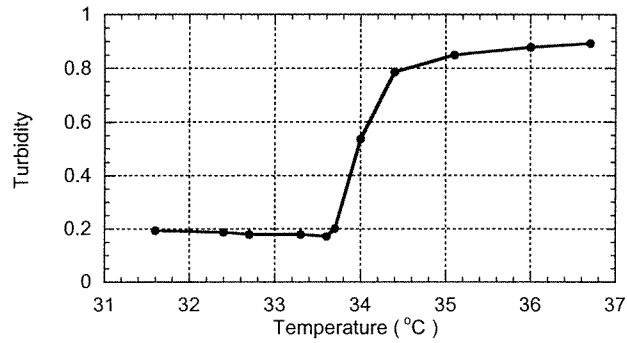
Figure 3. The turbidity of phantom 3 is plotted as a function of temperature. The low critical solution temperature is about 33 °C, at which the turbidity exhibits a sharp increase.
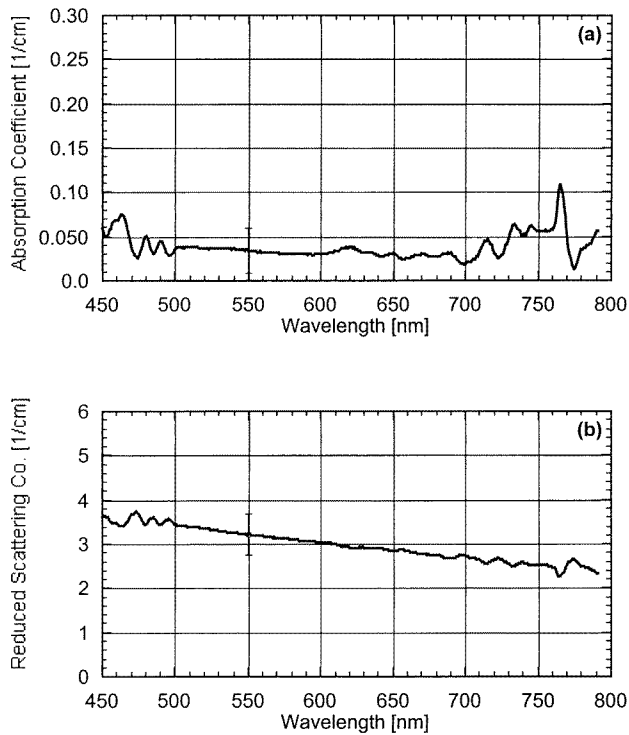
Figure 4. The average turbid optical properties of phantom 1 (PAAM:NIPA 1:0.1) at 60 °C. (*a*) The absorption coefficient, μ_a. (*b*) The reduced scattering coefficient, μ'_s. The standard deviation error bar is plotted at 550 nm.

of phantom 3 (PAAM:NIPA 1:0.5). The absorption coefficient between 500 and 700 nm was approximately 0.1 cm^{-1} (Figure 6(*a*)). The reduced scattering coefficient decreased very slightly with an increase in wavelength (figure 6(*b*)).

The increase of approximately 1 cm^{-1} in the reduced scattering coefficient of phantom 2 was probably caused by the interaction between the blue dextran and the NIPA/PAAM gel system. The reduced scattering coefficient of phantom 3 was larger than the first phantom, but
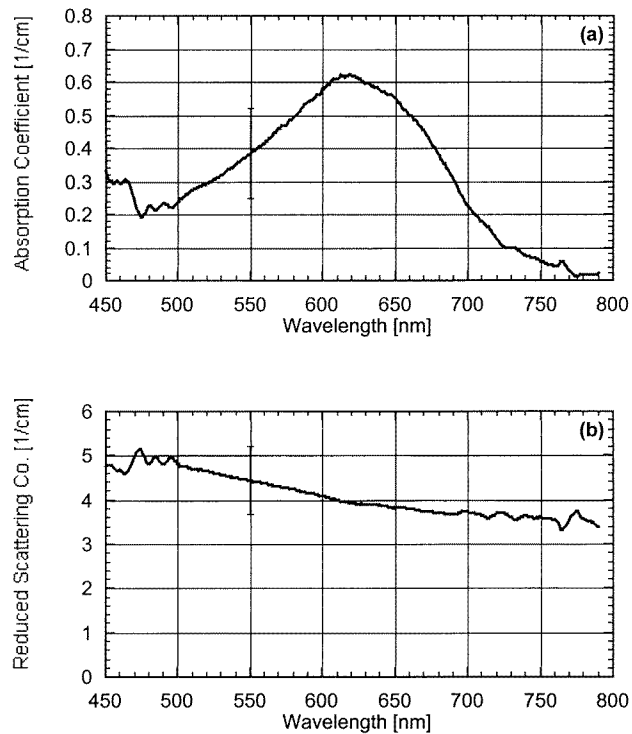
Figure 5. The average turbid optical properties of phantom 2 (PAAM:NIPA 1:0.1 with 0.05 g of blue dextran) at 60 °C. (*a*) The absorption coefficient, μ_a. (*b*) The reduced scattering coefficient, μ_s'. The standard deviation error bar is plotted at 550 nm.

was not five times larger than the concentration of NIPA. Finally, all three phantoms showed a similar trend in the reduced scattering spectra.

5. Discussion

As a tissue-simulating turbid medium, the NIPA/PAAM gel system exhibits the unique property that its turbidity can be tuned by adjusting the external temperature as shown in figure 3. Here, the PAAM gel network as a host matrix makes a negligible contribution to light absorption and scattering, and is insensitive to the temperature. The temperature-dependent turbidity change comes from the linear NIPA polymer chains that are entrapped inside the PAAM gel. When these NIPA chains are heated, the polymer molecular dimensions change abruptly from a state of well-solved random coils at temperatures below the LCST (33 °C) to a state of tightly packed globular particles at temperatures above. This is then followed by the onset of aggregation of individual polymer chains, mainly due to the intermolecular interaction between the hydrophobic groups distributed on the surface of the resulting globular particles of the polymer in an aqueous medium (Fujishige *et al* 1989). This spatial concentration fluctuation results in light scattering and an accompanying reduction in the transmission of visible light through the gel. The reduction in the transmission is quantified in terms of the sample turbidity. It is noted that the phase transition process between the transparent and the cloudy states in the NIPA/PAAM gel system is completely reversible as a function of temperature.
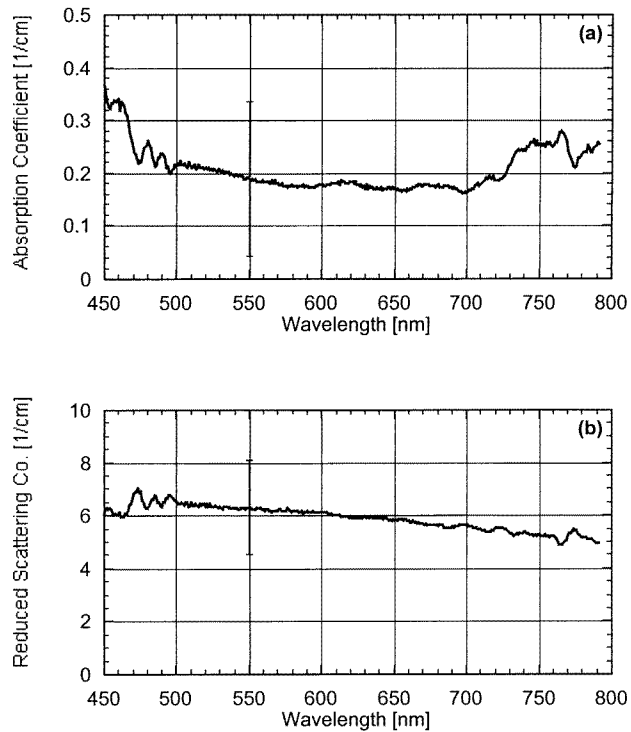
Figure 6. The average turbid optical properties of phantom 3 (PAAM:NIPA 1:0.5) at 60 °C. (*a*) The absorption coefficient, μ_a. (*b*) The reduced scattering coefficient, μ_s'. The standard deviation error bar is plotted at 550 nm.

The temperature-dependent turbidity of the NIPA entrapped system is similar to that of the free NIPA solution (Schild 1992) and the pure NIPA gel (Li *et al* 1995). However, the NIPA/PAAM gel undergoes the clear to cloudy transition near the LCST while its shape remains the same. In contrast, the NIPA solution does not have a shape, and the NIPA gel has to change its volume near the LCST. Therefore, the NIPA entrapped system is a better one for optical phantom applications.

The contribution of the NIPA polymer to the reduction of transmitted light is mainly through the light scattering mechanism, as revealed from the large scattering coefficient and the very small absorption coefficient (figures 4 and 6). An increase in the NIPA concentration can result in a substantial increase in the reduced scattering coefficient. To enhance the optical absorption of the NIPA/PAAM phantom, blue dextran is introduced into the system. As shown in figure 5, the NIPA/PAAM gel system with blue dextran indeed exhibits a larger absorption coefficient. However, we noticed a 1 cm^{-1} increase in the reduced scattering coefficient without changing the NIPA/PAAM concentration. This increase was probably caused by the interaction between the blue dextran and the NIPA/PAAM gel system. This problem can be solved by using one of several known absorbers that would not interact with the NIPA/PAAM gel system, for example Trypan blue dye or India ink. Also, the NIPA/PAAM gel system alone contains some absorption as shown in figure 4(*a*). And as shown in figure 6(*a*), increasing the concentration of NIPA five times also increases the absorption coefficient. Therefore, by selecting compositions of NIPA and blue dextran, or another absorber, the scattering coefficient and absorption coefficient of the NIPA/PAAM gel system can be adjusted

to simulate the optical properties of biological tissues at a specific wavelength. It is noted that the reduced scattering coefficient of the NIPA/PAAM gel system decreases with wavelength. This may indicate that the NIPA polymer chains aggregate to form clusters with a broad size distribution. When the wavelength becomes longer than the cluster sizes, the scattering coefficient decreases.

The collected spectra of the different collection fibres were found to be misaligned by 1 to 2 nm. We corrected this problem by aligning the characteristic spectral peaks of the collected spectra before the data fitting for optical properties. The peak finding procedure involved finding the characteristic spectral peak of the xenon lamp at 491 nm for every spectrum. All of the spectra from the collection fibres were aligned such that the characteristic peaks are at the same spectral location. Although the wavelength shift between the collection fibres was aligned, the extrapolated data showed artificial peaks between 450 and 500 and between 750 and 800 because the spectral peaks were not sharp. We have since improved the resolution of our system and thus improved our peak alignment.

The temperature-dependent turbidity of this new type of gel will find many applications in the optical stimulation of biological tissues. The optical properties of biological tissues are frequently found to vary dynamically. The variation of optical properties due to photocoagulation, mentioned earlier, is an example in laser therapeutics. The optical properties of haemoglobin vary with its oxygenation saturation, which is an important physiological parameter that changes with time or environment. The scattering coefficient of blood varies with the concentration of glucose because glucose modifies the refractive index of the interstitial fluid and thus changes the scattering cross section of the scatterers. When a device or a technique is developed for applications involving this type of dynamic parameter, a dynamically variable phantom such as the one developed in this research is highly desirable.

Dynamic phantoms may be useful in some other scenarios. Multiple static optical phantoms are sometimes made to check a device or technique for a range of optical properties; temperature-dependent optical phantoms may be used instead, where the optical properties can be varied with arbitrary resolution. A single dynamic phantom will cover a wide range of optical properties. Using a temperature field, one may produce a continuous distribution of optical properties in the phantoms, which would be difficult to accomplish using static phantoms. In all these examples and other possible uses, it should be pointed out that temperature control and monitoring are important issues when working around the LCST region due to the drastic change in turbidity. However, when working at a much higher temperature, as in our measurements, the need for temperature control is not as important because the temperature decay of the gel is slow.

6. Conclusion

As a possible candidate for use in tissue-simulating phantoms, the turbid optical properties of the NIPA/PAAM gel system were investigated using a multiwavelength oblique-incidence reflectometer. The turbidity of such a system can be easily changed by adjusting the sample temperature and NIPA concentration. It is found that the NIPA plays a crucial role in light scattering while the blue dextran determines the light absorption. The reduced scattering coefficient and the absorption coefficient of the NIPA/PAAM gel system can be adjusted to simulate the optical properties of biological tissues at a specific wavelength by choosing the compositions of NIPA and blue dextran.

Acknowledgments

References

Farrell T J, Patterson M S and Wilson B C 1992 A diffusion theory model of spatially resolved, steady-state diffuse reflectance for the non-invasive determination of tissue optical properties *in vivo Med. Phys.* **19** 879–88

Fujishige S, Kubota K and Ando I 1989 Phase transition of aqueous solutions of poly(*N*-isopropylacrylamide) and poly(*N*-isopropylmethacrylamide) *J. Phys. Chem.* **93** 3311

Li Y, Wang G and Hu Z 1995 Turbidity study of spinodal decomposition of an *N*-isopropylacrylamide gel *Macromolecules* **28** 4194

Lin S P 1996 Oblique-incidence fiber-optic reflectometry for measuring absorption and scattering in turbid media *MS Thesis* Rice University

Lin S P, Wang L H, Jacques S L and Tittel F K 1996 Measurement of absorption and scattering spectra with oblique incidence reflectometry *Advances in Optical Imaging and Photon Migration (OSA Technical Digest Series)* (Washington, DC: Optical Society of America) pp 44–9

——1997 Measurement of tissue optical properties by the use of oblique-incidence optical fiber reflectometry *Appl. Opt.* **36** 136–43

Marquez G and Wang L V 1997 White light oblique incidence reflectometer for measuring absorption and reduced scattering spectra of tissue-like turbid media *Opt. Express* **1** 454–60

Pickering J W, Prahl S A, Vanwieringen N, Beek J F, Sterenborg H J C M and van Gemert M J C 1993 Double-integrating-sphere system for measuring the optical properties of tissue *Appl. Opt.* **32** 339–410

Press W H, Flannery B P, Teukolsky S A and Veterlin W T 1992 *Numerical Recipes in C* 2nd edn (Cambridge: Cambridge University Press) section 15.5

Priest J H, Murray S L, Nelson J R and Hoffman A S 1987 Lower critical solution temperatures of aqueous copolymer: a thermal reversible, water-soluble, activated polymer for protein conjugation *Am. Chem. Soc. Symp. Ser.* **350** 255

Schild H G 1992 Poly(*N*-isopropylacrylamide) experiment, theory and application *Prog. Polym. Sci.* **17** 163

Schild H G and Tirrell D A 1990 Microcalorimetric detection of lower critical solution temperatures in aqueous polymer solutions *J. Phys. Chem.* **94** 4352

Tanaka T 1992 Phase transitions of gels *Am. Chem. Soc. Symp. Ser.* **480** 1

Taylor L D and Cerankowski L D 1975 Preparation of films exhibiting a balanced temperature dependence to permeation by aqueous solution—a study of lower consolute behavior *Polym. Sci., Pt. A: Polym. Chem.* **13** 2551

Wang L H and Jacques S L 1993 Analysis of diffusion theory and similarity relations *Proc. SPIE* **1888** 107–16

——1995 Use of a laser beam with an oblique angle of incidence to measure the reduced scattering coefficient of a turbid medium *Appl. Opt.* **34** 2362–6